Available online at www.sciencedirect.com
SCIENCE DIRECT®
Physica B 349 (2004) 76–83
PHYSICA B
www.elsevier.com/locate/physb

Density functional approach to study structural properties and electric field gradients in rare earth materials

S. Jalali Asadabadi[a], H. Akbarzadeh[b,*]

[a] Department of Physics, Faculty of Science, University of Isfahan (UI), Hezar Gerib Avenue, Isfahan 81744, Iran
[b] Department of Physics, Isfahan University of Technology, Isfahan 84154, Iran

Received 23 June 2003; received in revised form 16 December 2003; accepted 4 January 2004

Abstract

We investigated the effect of spin polarization on the structural properties and the electric field gradient (EFG) on Sn, In, and Cd impurities in RSn_3 (R = Sm, Eu, Gd) and RIn_3 (R = Tm, Yb, Lu) compounds. The calculations were performed self-consistently using the scalar-relativistic full potential linearized augmented plane wave method. The local density approximations and generalized gradient approximation (GGA) without spin polarization and with spin polarization (GGA + SP) to density functional theory were applied. In addition to that we performed some calculations within open core treatment (GGA + open core). It is clearly seen that GGA + SP is successful in predicting the larger lattice parameter and the dramatic drop of EFG for R = (Eu, Yb) relative to other rare-earth compounds.

PACS: 71.20.−b; 71.28.+d; 76.80.+y; 71.27.+a

Keywords: Electric field gradient; Strongly correlated systems; Rare earth; ^{111}Cd impurity; RSn_3; RIn_3; Hyperfine interaction

1. Introduction

The highly correlated f electrons in rare-earth materials have challenged the reliability of the results obtained by conventional density functional theory (DFT). It is generally believed that regular DFT in its local density approximations/generalized gradient approximation (LDA/GGA) formulation, without any modification, is insufficient to correctly deal with the f electrons; hence our understanding of the physical properties of these systems are often based on a many body model Hamiltonian or modified LDA such as LDA + U [1–3], LDA + SIC [4,5], and LDA + (open core) [6] approaches.

Strange et al. [5], by removing the spurious self-interaction of f electrons, reported a systematic investigation of the rare-earth elements and their sulfides. They confirmed the pre-claimed idea that there are two types of f electrons in these materials: Localized core-like f electrons that determine the valency, and delocalized band-like f electrons that are formed through hybridization with the s–d bands and which participate in bonding. The main

*Corresponding author. Tel.: +98-31-13912375; fax: +98-31-13912376.
E-mail address: akbarzad@cc.iut.ac.ir (H. Akbarzadeh).

0921-4526/$ - see front matter © 2004 Published by Elsevier B.V.
doi:10.1016/j.physb.2004.01.153

feature of their calculation was based on an f band splitting into two sub-bands: one occupied, and the other one unoccupied.

In a recent publication we investigated the valency of rare earths in RIn_3 (R = Sm, Eu, Gd) and RSn_3 (R = Tm, Yb, Lu), and calculated the electric field gradient (EFG) using DFT without spin polarization [7]. We found that since in regular DFT all f electrons are treated as band electrons, their densities of states are all located in a single peak at the Fermi level, which is not consistent with reality. We finally overcame this drawback by applying open-core approach.

The aim of the present work is to investigate the effect of spin polarization on the structural properties and the EFG of the same samples. Our objective is to investigate the borderline of LDA ability, that without any modification further than spin polarization we can obtain reliable results for some compounds with highly correlated f electrons. The organization of this paper is as follows. In Section 2 we present the calculational details. Section 3 deals with the results and discussions. Finally, we conclude this work with a summary in Section 4.

2. Calculational details

We utilize the full-potential linearized augmented plane wave (FP-LAPW) method within density functional theory. In this method wave functions, charge density, and potential are expanded in spherical harmonics within nonoverlapping muffin-tin spheres and in plane waves in the remaining interstitial region of the unit cell. As in the FP-LAPW method no shape approximation is introduced for potential and charge density, it is an appropriate procedure to obtain reliable results for the EFG with high sensitivity to anisotropic charge density distributions around the nucleus.

The EFG tensor is defined as the second derivative of the Coulomb potential with respect to the Cartesian coordinate at the nucleus, which is written as a traceless tensor. The Coulomb potential which is one of the crucial quantities of an accurate (full-potential) band structure calculation is given in LAPW as a lattice harmonics expansion inside the atomic spheres. In this representation, the required derivatives can be determined straightforwardly, and the largest component of the EFG tensor can be obtained directly from the $L = 2$, $M = 0$ component of the potential expansion inside the muffin-tin spheres [8]

$$V_{zz} = \sqrt{\frac{5}{4\pi}} \lim_{r \to 0} \frac{V_{20}}{r^2}. \quad (1)$$

It is assumed that the main axis of the EFG tensor points towards the z direction. The radial potential coefficient $V_{20}(r)$ near the nucleus ($r \to 0$) for a given charge density is obtained numerically by solving Poisson's equation using a method proposed by Weinert [9].

The calculations were performed using the WIEN97 code developed by Blaha and coworkers [10], which has been successfully applied to a wide range of systems. In this code, core and valence states separated by their energy are treated differently. Core states are treated within a multi-configuration relativistic Dirac–Fock approach, while valence states are treated only in a scalar relativistic approach, except for $EuSn_3$ for which the valence states were calculated self-consistently in second-order variational steps taking spin–orbit coupling into account. In the latter case, the number of symmetry operations was reduced from 48 to 16 by assuming the z-direction to be a preferentional direction of the spin coupled to the orbit. It was shown that by including the spin–orbit interaction the results do not change substantially. Since the incorporation of this coupling is very time consuming, it was neglected throughout the calculation. For better treatment of the core electrons we decomposed them into high-lying semicore and deeper true core states. As the electronic charge of semicore states are not completely confined inside the respective muffin-tin spheres, we treated them as band states in the full (nonspherical) potential. For these states, in addition to the usual LAPW basis, we included local orbitals to increase the flexibility of the basis set [11], and to be able to use a sufficiently fine k sampling. This procedure results in a more accurate calculation of the EFG, which is extremely sensitive to the basis set [12]. The true core

states were treated atomic like in the self-consistent muffin-tin potential. In our calculations, electronic states with an energy of at least 6 Ry below the Fermi energy were considered as true core states. For the muffin-tin radius of the rare-earth elements as well as of Sn and In, a value of 2.65 a.u. was chosen throughout, while for the Cd impurity manipulated into the RSn_3/In_3 compounds a radius of 2.5 a.u. was used. The maximum angular momentum quantum number l as a cutoff for expanding the Kohn–Sham wavefunctions in terms of lattice harmonics inside the muffin-tin spheres was confined to $l_{max} = 12$.

The potential and charge density was expanded inside the atomic spheres in crystal harmonics up to $L = 6$. The wave functions in the interstitial region were expanded in plane waves with a cutoff of $K_{max} = 7/R_{MT}$, where R_{MT} was the smallest muffin-tin radius in the unit cell. The periodic charge density and potential were Fourier expanded up to $G_{max} = 16$. We adjusted the value of the mixing parameter of the charge density to 0.1, and used Broyden's scheme. We have taken a mesh of 165 special k points to implement the valence state integration in the irreducible wedge of the Brillioun zone (BZ) that corresponds to the grids $18 \times 18 \times 18$ in the scheme of Monkhorst–Pack [13]. The mesh of k points, charge density and potential expansion cutoff and finally muffin-tin radii were allowed to vary for ensuring the convergence. The exchange–correlation energy was calculated within the LDA based on the Perdew–Zunger parameterization [14], with and without including advanced GGA using Perdew–Burke–Ernzerhof parameterization [15], and with and without considering spin polarization. For spin polarized calculations, a ferromagnetic moment was imposed on R at the start of the self-consistency cycle. As for some compounds, this is not the true magnetic order [16], such an assumption should be considered as an extra possible source of error. At the end of the self-consistency cycle, $YbIn_3$ and $LuIn_3$ came out to be nonmagnetic, all others remained ferromagnetic. In order to calculate the EFG at the Cd site as a representation of an impurity atom in each compound, all sides of the unit cell were doubled to construct a supercell with 16 atoms [7]. Further increase of the sides of the supercell did not change the results significantly. To keep the same accuracy with the previous primitive unit cell, the mesh of k points in the supercell was reduced to 75 corresponding to the $9 \times 9 \times 9$ grids. The energy for each orbital in $EuSn_3$, and in $YbIn_3$ is linearized by selecting the most probable energy calculated for each density of state over the valence and semicore energy windows. The linearizations obtained for $EuSn_3$ and $YbIn_3$ are then used as an initial input for the $SmSn_3$, $GdSn_3$, and the $TmIn_3$, $LuIn_3$, respectively, and we allow the program to search automatically for the best-linearized energies of Cd orbitals and check whether they are perfect.

3. Results and discussion

3.1. Structural properties

By calculating the total energy of a primitive unit cell as a function of its volume and fitting the data with the Birch equation of state [17] we obtained the lattice parameters, bulk moduli, and the pressure derivative of the bulk moduli for RSn_3 (R = Sm, Eu, Gd) and RIn_3 (R = Tm, Yb, Lu) by LDA, GGA, GGA + SP, GGA + open core (valence 2, 2.5 and 3) approaches. These results along with the experimental data are listed in Tables 1 and 2. The lattice parameters calculated by GGA for all compounds are in

Table 1
The comparison of the measured lattice parameters in Å at $T = 300$ K with the theoretical values calculated at $T = 0$ K within LDA, GGA without spin polarization (GGA), GGA with spin polarization (GGA + SP), and GGA + open core (valence 2, 2.5, 3)

	$SmSn_3$	$EuSn_3$	$GdSn_3$	$TmIn_3$	$YbIn_3$	$LuIn_3$
LDA	4.529	4.515	4.513	4.434	4.443	4.434
GGA	4.654	4.649	4.648	4.589	4.594	4.566
GGA + SP	4.708	4.715	4.683	4.593	4.594	4.566
GGA^{divalent}	4.809	4.784	4.749	4.651	4.626	4.655
GGA$^{di\ \&\ half\ valent}$	—	4.758	4.733	4.619	4.604	—
GGA^{trivalent}	4.747	4.732	4.717	4.587	4.582	4.576
[a]Expt.	4.69	4.75	4.68	4.56	4.61	4.55

[a] Ref. [16,20].

Table 2
The calculated bulk modulus in GPa and its pressure derivative within LDA, GGA without spin polarization (GGA), and GGA with spin polarization (GGA + SP)

	$SmSn_3$	$EuSn_3$	$GdSn_3$	$TmIn_3$	$YbIn_3$	$LuIn_3$
B_0(LDA)	65.517	59.786	62.549	73.032	70.596	77.468
B'_0(LDA)	2.509	2.312	2.948	5.789	5.089	4.708
B_0(GGA)	63.531	61.020	59.629	53.440	55.180	62.604
B'_0(GGA)	3.478	3.401	3.560	4.937	4.486	4.159
B_0(GGA + SP)	58.011	54.239	64.318	55.788	55.081	62.648
B'_0(GGA + SP)	4.354	5.064	4.688	4.709	4.402	4.155

better agreement with the experiment than those obtained by LDA. The better prediction of experimental results by GGA has also been observed in most rare-earth metals and is believed to be due to the fact that the nonlocality of exchange and correlation is better taken into account by GGA than LDA [18]. We expect the lattice constant for divalent Eu and Yb to be higher than those of the other rare-earth compounds. The divalent character results in weaker interatomic bonds and manifests itself in a higher lattice parameter and also compressibility, which is the inverse of bulk modulus. It is clearly seen that GGA fails to predict such behavior for Eu compounds, while GGA + SP improves the results in the right direction. By comparing the charge densities belonging to nonmagnetic and polarized solutions of 4f electrons of gadolinium atom, Richter [6] has illustrated a clear reason why spin-independent DFT is not suited to magnetic systems. Our results confirm his conclusions. As expected, due to the rather full f shell in Lu, Yb and even Tm compounds, spin polarization does not practically affect their lattice parameter. For $SmSn_3$ and $GdSn_3$ the results obtained by GGA + SP are in nice agreement with the experiment, while for Eu and Yb compounds the results obtained by open core calculation with a mixed valence ($\sim$2.5) are in better agreement with experiment. A point worth to mention is that the deviations of the lattice parameter calculated by GGA + SP and GGA + open core are more significant in Sm, Eu, and Gd compounds compared to Tm, Yb, and Lu compounds. It is probably because of the fact that going from left to right in the list of lantanides the f electrons are getting more localized. Hence, for the highly localized f electrons in Tm, Yb, and Lu compounds it does not make any difference whether we leave them alone or confine them inside the core by open core approach. Similar behavior has been predicted for f electrons in actinides [19]. Finally, it should be noticed that although the equilibrium lattice parameters can be accurately extracted by fitting the total energy-volume data with an appropriate equation of state, the value obtained for the bulk modulus and its pressure derivative are sensitive to the range of fitting. Hence, for the results presented in Table 2 only the qualitative analysis is reliable and we cannot fully trust the quantitative values. Furthermore, as, to our knowledge, no experimental data for the bulk modulus and its derivative have been reported yet, our results serve only as a prediction for future studies.

3.2. Electric field gradient

In the literature, different conversion relations analyze the experimental results of the nuclear quadrupole interaction. Then, to compare our calculated EFG with experiment, we first need to specify the conversion relation that has been used. The experimental data to calculate the EFG on the Sn site of RSn_3 (R = Sm, Eu, Gd) compounds are obtained from Mössbauer spectroscopy. Hence the value of V_{zz} can be calculated from the measured Doppler velocity Δ_v via

$$V_{zz}[10^{21}\ \mathrm{V\,m^{-2}}] = 12.79\Delta_v\ (\mathrm{mm\,s^{-1}}). \quad (2)$$

The EFG values on a Cd impurity substituted at Sn and In sites were obtained by perturbed angular correlation measurements with the following conversion relation:

$$V_{zz}[10^{21}\ \mathrm{V\,m^{-2}}] = \frac{0.041355}{Q(b)}\omega\ (\mathrm{MHz}). \quad (3)$$

We used the recently proposed value of $Q = 0.83b$ for the nuclear quadrupole moment of Cd.

The calculated EFG on Sn sites of RSn_3 (R = Sm, Eu, Gd) are compared with the experimental data in Table 3. For all compounds, the less agreement with the experiment is due to LDA calculations. GGA + SP correctly predict the lower

Table 3
The comparison of the derived EFG in 10^{21} V/m^2 from the measured quadrupole interactions of ^{119}Sn ($Q = 0.124, E_0 =$ 23.8 keV) at $T = 77$ K and 4.2 K with the theoretical values calculated at $T = 0$ K within LDA, GGA without spin polarization (GGA), and GGA with spin polarization (GGA + SP)

	$SmSn_3$	$EuSn_3$	$GdSn_3$
LDA	17.49	16.56	16.51
GGA	16.71	15.35	15.39
GGA + SP	15.20	14.03	15.20
[a]Expt.$^{T=4.2\ K}$	13.82	13.56	—
[a]Expt.$^{T=77\ K}$	13.82	11.64	13.56

[a] Ref. [16].

Table 4
The comparison of the derived EFG in 10^{21} V/m^2 from the measured quadrupole coupling constants of ^{111}Cd ($Q = 0.83b$, $E_0 = 247$ keV) at $T = 300$ K and 4.2 K with the theoretical values calculated at $T = 0$ K within GGA without spin polarization (GGA), and GGA with spin polarization (GGA + SP)

	$SmSn_3$	$EuSn_3$	$GdSn_3$	$TmIn_3$	$YbIn_3$	$LuIn_3$
GGA	4.06	3.44	3.64	3.36	3.11	6.08
GGA + SP	2.62	1.81	3.76	3.49	3.12	6.08
[a]Expt.$^{T=300\ K}$	2.12	0.63	2.12	4.37	1.92	4.32
[a]Expt.$^{T=4.2\ K}$	—	—	—	—	2.16	—

[a] Ref. [20].

value of EFG in $EuSn_3$ compared to the other two compounds which is consistent with the experimental results obtained at nonzero temperatures. As EFG is very sensitive to the charge density around the nucleus, its nearly constant value at Sn sites for all three compounds confirms the argument presented in Ref. [16] that the charge densities around a Sn nucleus are rather identical and independent of the rare-earth atoms. In Table 4 we compare the calculated EFG on a Cd impurity with experiment [20]. Here also, the results obtained by GGA + SP are in better agreement with the experiment. The EFG drop for Eu and Yb compounds, attributed to a changing valency, is clearly visible. The small deviation between calculation and experiment presented in Tables 3 and 4 are not unexpected given the uncertainties of the temperature effect, which are not included in our calculation. It seems that the electric field gradient at most cases decreases when the temperature rises. The EFG measured in $YbIn_3$ and $EuSn_3$ at two different temperatures given in Tables 3 and 4 confirm this expectation. In addition to that, to avoid time-consuming, we have not relaxed the atomic position. Since EFG may strongly be affected by local geometry, the relaxation of the atoms from their original lattice positions can alter their value [21]. Hence, the atomic fixation can be considered as an another source of error in our calculation. The last possible source of error is that in the EFG calculations we have used experimental lattice parameters, thus with values which are not identical to those obtained from E–V curves. We will show later that the effect of this discrepancy is ignorable.

At this stage we raise a question that our ab initio study is going to answer. To which extent is the EFG at X in a RX_3 compound sensitive to the behavior of f electrons in R and how can the spin polarization push the system in the right direction? In order to tackle this question, we will follow Ref. [7] by introducing a visualization tool called anisotropy function $\Delta p(E)$. This function allows us a transparent interpretation of the qualitative behavior of V_{zz}. As V_{zz} expresses the deviation from spherical symmetry of the electron density in the environment of X, this asphericality is given in terms of p-orbitals (s and d orbitals have ignorable effects [7]) by the following expression:

$$V_{zz} \approx V_{zz}^{p}, \tag{4}$$

$$V_{zz}^{p} = \Delta p(E_{\mathrm{F}}) \left\langle \frac{1}{r^3} \right\rangle_{p}, \tag{5}$$

$$\Delta p(E_{\mathrm{F}}) = \tfrac{1}{2} p_{xy}^{\mathrm{I}}(E_{\mathrm{F}}) - p_{z}^{\mathrm{I}}(E_{\mathrm{F}}), \tag{6}$$

$$p_i^{\mathrm{I}}(E_1) = \int_{-\infty}^{E_1} p_i(E)\, \mathrm{d}E. \tag{7}$$

Here $\langle 1/r^3 \rangle_{\mathrm{p}}$ is an expectation value for the p-orbitals, $p_z(E)$ is the partial p-DOS (DOS, Density of states) in the muffin-tin sphere around an atom, and E_{F} is the Fermi energy. The integral $p_i^{\mathrm{I}}(E_1)$ counts the number of p_i electrons in a muffin-tin sphere with energy less than E_1.

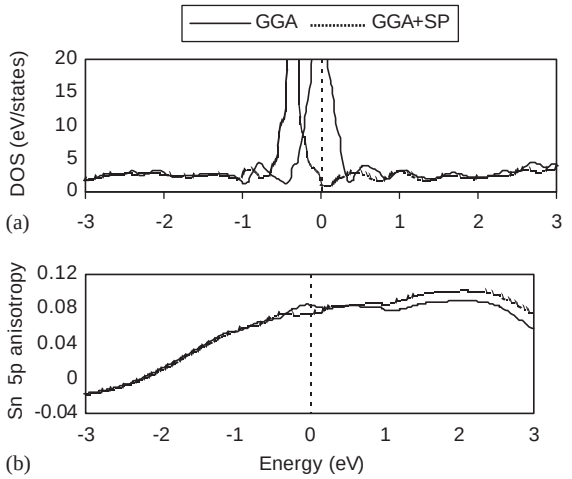

Fig. 1. All graphs are for $EuSn_3$. The solid line is for GGA, and faint line for GGA + SP. (a) total DOS, (b) Sn 5p anisotropy function.

Table 5
The decompositions of calculated EFGs at Cd, Sn and In sites into the valence EFG for spin up and down and the total lattice EFG in 10^{21} V/m^2

	V_{zz}^{latt}	${}^{\mathrm{val}}V_{zz}$	${}^{\mathrm{val}}V_{zz}^{\uparrow}$	${}^{\mathrm{val}}V_{zz}^{\downarrow}$
		Cd		
$SmSn_3$	−0.03	2.62	2.26	0.39
$EuSn_3$	−0.03	1.81	1.49	0.35
$GdSn_3$	−0.04	3.76	2.18	1.62
$TmIn_3$	−0.03	3.49	1.70	1.82
$YbIn_3$	−0.00	3.12	1.56	1.56
$LuSn_3$	−0.02	6.08	3.05	3.05
		Sn		
$SmSn_3$	−0.02	15.02	8.49	6.73
$EuSn_3$	−0.03	14.03	7.33	6.73
$GdSn_3$	−0.02	15.83	7.39	8.46
		In		
$TmIn_3$	−0.01	8.95	4.22	4.74
$YbIn_3$	−0.01	8.34	4.18	4.18
$LuIn_3$	−0.04	11.23	5.62	5.62

In order to investigate the effect of spin polarization on the EFG value, the total DOS of $EuSn_3$ within GGA and GGA + SP are shown in Fig. 1a. The only considerable effect of spin polarization is the shift of the f-peak from the initial Fermi level to the left. Due to the hybridization of f electrons on R sites with p electrons on neighboring X cites, the shift of the f peak affects P_{xy} and P_z and subsequently $\Delta p(E_F)$. The changes of the anisotropy function with energy are shown in Fig. 1b. It is clearly seen that $\Delta p(E_F)$ and, as a result of that, the EFG obtained by GGA + SP are lower than the corresponding values within GGA.

To analyze the origin of the EFG on Cd, Sn, and In sites, we decomposed the calculated EFG into several different contributions (Table 5). The valence EFG (${}^{\mathrm{val}}V_{zz}$) originates from the asphericity of the valence (and semicore) charge density inside the muffin-tin sphere. The lattice EFG (${}^{\mathrm{lat}}V_{zz}$) arises from the boundary value problem and charge distribution outside the muffin-tin sphere. ${}^{\mathrm{val}}V_{zz}$ is further decomposed into spin-up (${}^{\mathrm{val}}V_{zz}^{\uparrow}$) and spin-down (${}^{\mathrm{val}}V_{zz}^{\downarrow}$) contributions. It is seen that the lattice contribution is negligibly small (less than 2% of the total EFG), which reflects the fact that the main origin of the EFG lies in the deviation from spherical symmetry of the valence charge density near the nucleus. It also confirms that the total EFG is not highly sensitive to the lattice parameters. Hence, the nonoptimized experimental lattice constant used in our calculation is acceptable. ${}^{\mathrm{val}}V_{zz}^{\uparrow} - {}^{\mathrm{val}}V_{zz}^{\downarrow}$ is expected to be a qualitative criterion for magnetism of the system; the vanishing of this quality for non-magnetic compounds such as $YbIn_3$ and $LuIn_3$ confirms this expectation.

In order to analyze the up and down contributions to V_{zz} on Cd, Sn and In in the listed compound we concentrate, as an example, on the Sn site in $EuSn_3$. The spin-up and down DOS and their corresponding p_z and p_{xy} on Sn sites are shown in Fig. 2. First of all, it is seen that spin polarization has split the up and down f peaks (Fig. 2a and b). This feature is compatible with reality. In nature there are two types of f electrons, localized and nonlocalized, and as a result of that, the f band should split into two sub-bands. In regular GGA, as the strong correlation between the f electrons are not treated properly, all of them are located in a single peak at E_F. Hence, it is not unjustified to expect that magnetism pushes the system in the right direction. How does the f-peak splitting affect p_z, p_{xy}, $\Delta p(E_F)$, and consequently EFG? Fig. 2c and d show the changes of p_z and p_{xy} with energy for up and down spin separately.

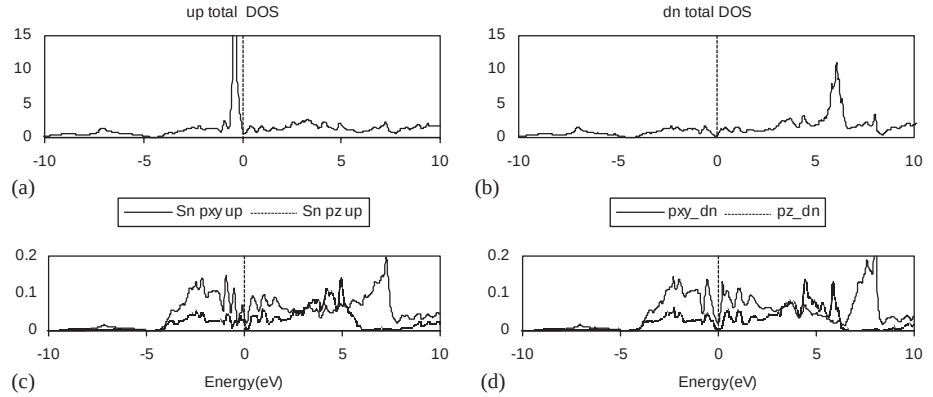

Fig. 2. All graphs are for $EuSn_3$. (a) total spin-up DOS, (b) total spin-down DOS. The changes of p_z (faint curves) and p_{xy} (solid curves) as a function of energy are shown in (c) for spin-up and in (d) for spin-down.

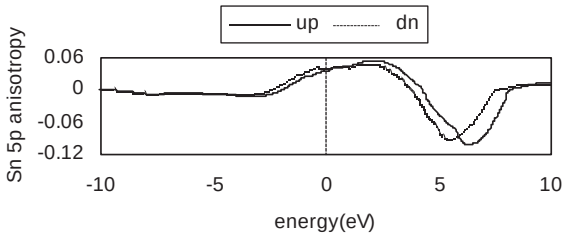

Fig. 3. The changes of anisotropy function $\Delta p(E)$ for both up (faint) and down (solid) spin directions with respect to energy.

Below -4 eV the two sets of curves coincide. In the region $[-4, 0]$ eV $P_{xy}^{\uparrow}$ is slightly larger than $P_{xy}^{\downarrow}$. This difference is more visible at around -1 eV, which is the location of the $f^{\uparrow}$ peak. One can conclude that the Sn $p^{\uparrow}$-electrons in the xy-plane hybridize with the f-electrons of the neighboring rare-earths (which are all 4 in the xy-plane). In Fig. 3 the anisotropy function $\Delta p(E)$ is given for two spin directions (say, $\Delta p^{\uparrow}(E)$ and $\Delta p^{\downarrow}(E)$). At the Fermi level, $\Delta p^{\uparrow}(E)$ is slightly larger than $\Delta p^{\downarrow}(E)$. Exactly the same was seen for V_{zz} in Table 3, which demonstrates once more that the p-anisotropy really reflects the behavior of V_{zz}. As we already expected from p_z and P_{xy} curves, no difference is observed between the two curves below -4 eV. In the region $[-4, 0]$ $\Delta p^{\uparrow}(E)$ is larger than $\Delta p^{\downarrow}(E)$, and at around -1 eV $p^{\uparrow}$ the anisotropy shows a clear peak. This is due to the $f^{\uparrow}$ peak located in this area.

4. Conclusion

We employed the FP-LAPW method to calculate the structural properties of RSn_3 (R = Sm, Eu, Gd) and RIn_3 (R = Tm, Yb, Lu) by LDA, GGA, GGA + SP, and GGA + open core (valence 2, 2.5, and 3) approaches. For Eu and Yb compounds open core and for other compounds GGA + SP results are in better agreement with the experiment. We also calculated the EFG at Sn, In, and impurity Cd sites in RSn_3 (R = Sm, Eu, Gd) and RIn_3 (R = Tm, Yb, Lu) compounds. Here also, the results obtained by GGA + SP are in better agreement with the experiment. The reasonable agreement of the results calculated by GGA + SP with the experiment is an indication that even for such highly correlated systems the spin splitting introduced by magnetism can partly describe the strong Coulomb correlation. However, we have to notice that the LSDA as an approach with self-interaction has a limited justification to be applied for localized states.

Acknowledgements

The authors acknowledge the financial support of the Isfahan University of Technology and also the Association Scheme of the Abdus Salam International Centre for Theoretical Physics

(ICTP). They are also grateful to S. Cottenier for his useful discussions.

References

[1] P. Novak, F. Boucher, P. Gressier, P. Blaha, K. Schwarz, Phys. Rev. B 63 (2001) 235114.
[2] D.L. Price, B.R. Cooper, Say-Peng Lim, I. Avgin, Phys. Rev. B 61 (2000) 9867.
[3] V.I. Anisimov, F. Aryasetiawan, A.I. Lichtenstein, J. Phys.: Condens. Matter 9 (1997) 767.
[4] A. Svane, W.M. Temmerman, Z. Szotek, L. Petit, P. Strange, H. Winter, Phys. Rev. B 62 (2000) 13394.
[5] P. Strange, A. Svane, W.M. Temmerman, Z. Szotek, Nature 399 (1999) 756.
[6] M. Richter, J. Phys. D 31 (1998) 1017.
[7] S.J. Asadabadi, S. Cotteneer, H. Akbarzadeh, R. Saki, M. Rots, Phys. Rev. B 66 (2002) 195103.
[8] P. Blaha, K. Schwarz, P.H. Dederichs, Phys. Rev. B 37 (1988) 2792.
[9] M. Weinert, J. Math. Phys. 22 (1981) 2433.
[10] P. Blaha, K. Schwarz, J. Luitz, WIEN97, A full potential linearized augmented plane wave package for calculating crystal properties, Karlheinz Schwarz, Tech. Univ. Wien, Vienna, 1999. (ISBN 3-9501031-0-4); Updated version of P. Blaha, K. Schwarz, P. Sorantin, S.B. Trickey, Comp. Phys. Commun. 59 (1990) 399. In this work, version 97.10 was used.
[11] D.J. Singh, Phys. Rev. B 43 (1991) 6388.
[12] E.L. Bominaar, J. Guillin, A. Sawayn, A.X. Traufuxen, Phys. Rev. B 39 (1989) 72.
[13] H.J. Monkhurst, J.D. Pack, Phys. Rev. B 13 (1976) 5188.
[14] J.P. Perdew, A. Zuanger, Phys. Rev. B 23 (1981) 5048.
[15] J.P. Perdew, S. Burke, M. Ernzerhof, Phys. Rev. Lett. 77 (1996) 3856.
[16] J.P. Sanchez, J.M. Friedt, G.K. Shenoy, A. Percheron, J.C. Achard, J. Phys. C 9 (1976).
[17] F. Birch, J. Geophys. Res. 83 (1978) 1257.
[18] A. Delin, L. Fast, B. Johanson, Phys. Rev. B 8 (1998) 58.
[19] L. Petit, A. Svane, W. M. Temmerman, Z. Szotek, Phys. Rev. B 63 (2001) 165107.
[20] G.P. Schwartz, D.A. Shirley, Hyperf. Interact. 3 (1977) 67.
[21] S. Lany, P. Blaha, J. Hamann, V. Ostheimer, H. Wolf, T. Wichert, Phys. Rev. B 62 (2000) 2259.